Appl. Phys. A (2007)
DOI: 10.1007/s00339-007-3942-8

Applied Physics A
Materials Science & Processing

Invited paper

Z.L. WANG

Novel nanostructures of ZnO for nanoscale photonics, optoelectronics, piezoelectricity, and sensing

School of Materials Science and Engineering, Georgia Institute of Technology, Atlanta, GA 30332-0245, USA

Received: 3 October 2005/Accepted: 13 January 2007

ABSTRACT Wurtzite-structured semiconductors such as ZnO, GaN, AlN, CdSe and ZnS are important materials for nanoscale devices. Zinc oxide, for example, is a unique material that exhibits semiconducting, piezoelectric, and pyroelectric properties. Using a solid–vapor phase thermal sublimation technique, nanocombs, nanorings, nanohelixes/nanosprings, nanobows, nanobelts, nanowires, and nanocages of ZnO have been grown under specific growth conditions. This paper is about the synthesis, structure, growth mechanisms, and potential applications of these nanostructures in optoelectronics, sensors, transducers, and biomedical science.

PACS 81.07.-b; 78.67.-n; 85.35.-p

1 Introduction

Since the discovery of oxide nanobelts of semiconducting oxides in 2001 [1], research in one-dimensional (1D) nanostructures of functional oxide has attracted a great attention due to their unique and novel applications in optics, optoelectronics, catalysis, and piezoelectricity. Semiconducting oxide nanobelts are a unique group of quasi one-dimensional nanomaterials that have been systematically studied for a wide range of materials with distinct chemical composition and crystallographic structures [2, 3]. Field-effect transistors [4] and ultra-sensitive nanosize gas sensors [5], nanoresonators [6] and nanocantilevers [7] have been fabricated based on individual nanobelts. Thermal transport along a single nanobelt has been measured [8]. Very recently, nanobelts, nanosprings [9], and nanorings [10] that exhibit piezoelectric properties have been synthesized, which could be a candidate for nanoscale traducers, resonators, and sensors.

Wurtzite structure [11] is a unique family for functional materials, whose members include (but are not limited to) ZnO, GaN, AlN, CdSe, and ZnS. Owing to the non-centrosymmetric structure, the wurtzite family is unique for piezoelectricity and pyroelectricity. Zinc oxide (ZnO) is a versatile smart material that has key applications in catalysts, sensors, piezoelectric transducers [12], transparent conductor [13], and surface acoustic wave devices [14]. The structure of ZnO, for example, can be described as a number of alternating planes composed of tetrahedrally coordinated O^{2-} and Zn^{2+} ions, stacked alternatively along the *c*-axis (Fig. 1a). The oppositely charged ions produce positively charged Zn-(0001) and negatively charged O-$(000\bar{1})$ polar surfaces, resulting in a normal dipole moment and spontaneous polarization along the *c*-axis (Fig. 1b). If the elastic deformation energy is largely suppressed by reducing the thickness of a nanobelt, the polar nanobelt could self-assembly into different shapes as driven by minimizing the electrostatic energy coming from the ionic charges on the polar surfaces (Fig. 1c and d), analogous to the charge configurations of a RNA molecule. This review focuses on the formation of various nanostructures of ZnO, aiming at showing their structures, growth mechanisms, and potential applications in optoelectronics, sensors, transducers, and biomedical science.

2 Growth of novel nanostructures

2.1 *Nanobelts, nanowire arrays, and nanotubes*

Nanobelts are nanowires that have a well-defined geometrical shape and side surfaces. By sublimation of ZnO powder without introducing catalyst, nanobelts of ZnO are grown [1]. Figure 2a shows a TEM image of ZnO nanobelts where each nanobelt has a uniform width along its entire length. No particle was observed at the end of the nanobelt. The nanobelt has specific growth direction and side surfaces. Nanobelts of more than 20 different materials have been grown [15, 16].

Figure 2b shows an SEM image of uniform ZnO nanorods/nanowires grown using Au catalyst on a single-crystal alumina substrate [17]. The nanorods are aligned and their distribution is determined by the locations of the Au catalyst. The nanorods grow along [0001] and their side surfaces are enclosed by $\{2\bar{1}\bar{1}0\}$. The aligned nanorods have applications in field emission and bio-fluid transport.

Like many other materials, hexagonal tubular structure of ZnO has also been found. Figure 2c shows a ZnO nanotube, which is along [0001] and enclosed by six facets [18]. The nanotube is believed to be formed first as a Zn rod. Surface

✉ Fax: 1-404-894-8008, E-mail: zhong.wang@mse.gatech.edu

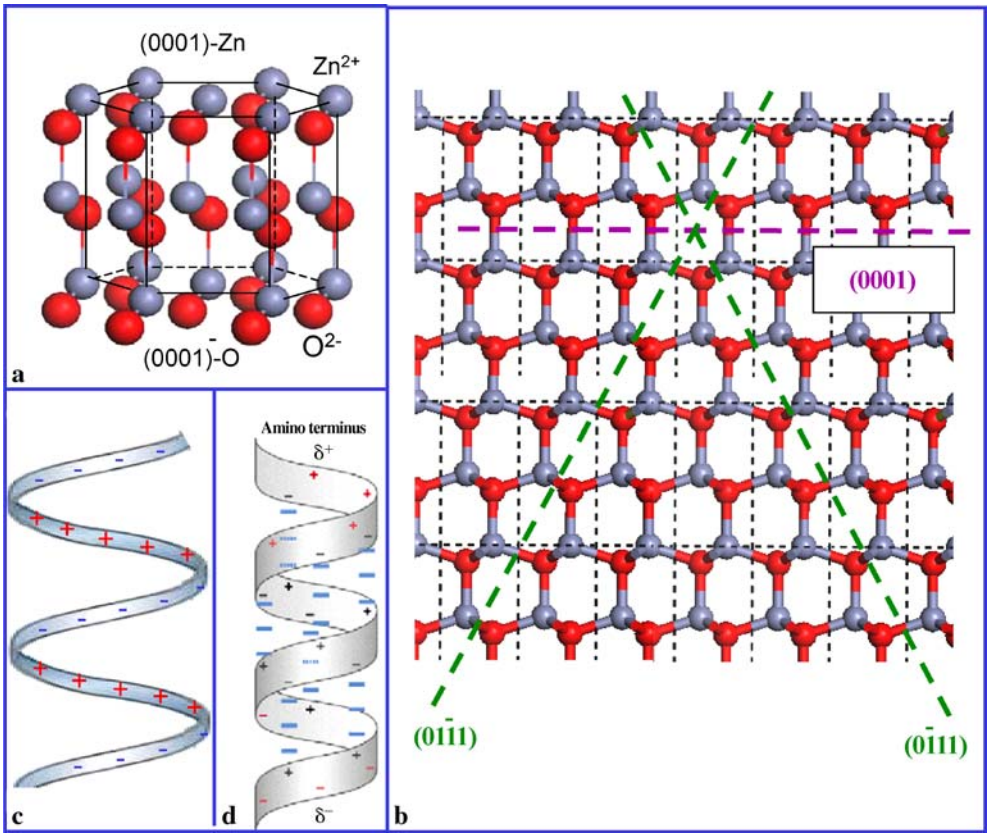

FIGURE 1 (**a**) Structural model of ZnO. (**b**) The projected structure of ZnO along *a*-axis, showing the {0001} and {01$\bar{1}$1} polar surfaces. (**c**) Spiral model of ZnO polar nanobelt. (**d**) Charge model of an RNA molecule

oxidation forms a ZnO shell and then a sublimation of the Zn core results in a hollow ZnO tube.

2.2 *Nanopropellers*

Modifying the composition of the source materials can drastically change the morphology of the grown oxide nanostructure. We used a mixture of ZnO and SnO_2 powders in a weight ratio of 1:1 as the source material to grown a complex ZnO nanostructure [19]. Figure 2d shows an SEM image of the as-synthesized products with a uniform feature consisting of sets of central axial nanowires surrounded by radically distributed branches. The growth of the novel structure presented here can be separated into two stages. The first stage is a fast growth of the ZnO axial nanowire along [0001]. The growth rate is so high that a slow increase in the size of the Sn droplet has little influence on the diameter of the nanowire and thus the axial nanowire has a fairly uniform shape along the growth direction. The second stage of growth is the nucleation and epitaxial growth of the nanoribbons due to the arrival of the tiny Sn droplets onto the ZnO nanowire surface. This stage is much slower than the first because the lengths of the nanoribbons are uniform and much shorter than that of the nanowire.

2.3 *Mesoporous single-crystal structured* ZnO *nanowire*

Mesoporous structures are usually composed of amorphous or polymer materials and the porosity is achieved by solvent-based organic or inorganic reactions. There are few reports on mesoporous structures of crystalline materials. Recently, we have found that single-crystal structured ZnO nanowire can have mesoporous walls/volumes (Fig. 2e) [20]. The high porous ZnO nanowires are also enclosed epitaxially by a thin layer of Zn_2SiO_4 at the exterior surface, which is formed during the synthesis with the use of a silicon substrate. The nanowires are single crystals and grow along [0001]. The thermal decomposition of ZnO and the formation of an uncontinuous Zn_2SiO_4 network on the surface of the nanowire are likely to be the key for forming the high-porosity volume. This technique reveals a new approach for fabricating high-porosity nanowires as well as a composite of ZnO-Zn_2SiO_4 luminescence materials. These unique structures exhibit a very high surface-to-volume ratio and are expected to have high capacity and particular selectivity that could be applied to filter and sensor systems.

2.4 *Nanocage and hierarchical structures*

By changing the composition of the source material, nanocages of ZnO shells have been grown [21]. A mixture of commercial ZnO, SnO_2 and graphite powders in atomic ration of 2:1:1 was used as the source materials. ZnO balls and polyhedra are observed (Fig. 2f). The polyhedron is enclosed by (0001) (top and bottom surface), {10$\bar{1}$0} (side surfaces), stepped {10$\bar{1}$1} (inclined surfaces) and high index planes with rough surfaces. A common feature is that the shell exhibits mesoporous structure. Although the polyhedral shell structure appears to be composed of nanocrystals, transmission electron diffraction and imaging indicates that they have a "single-crystalline" textured orientation, and the side surfaces are {10$\bar{1}$0}. The nanocage is formed from a Zn

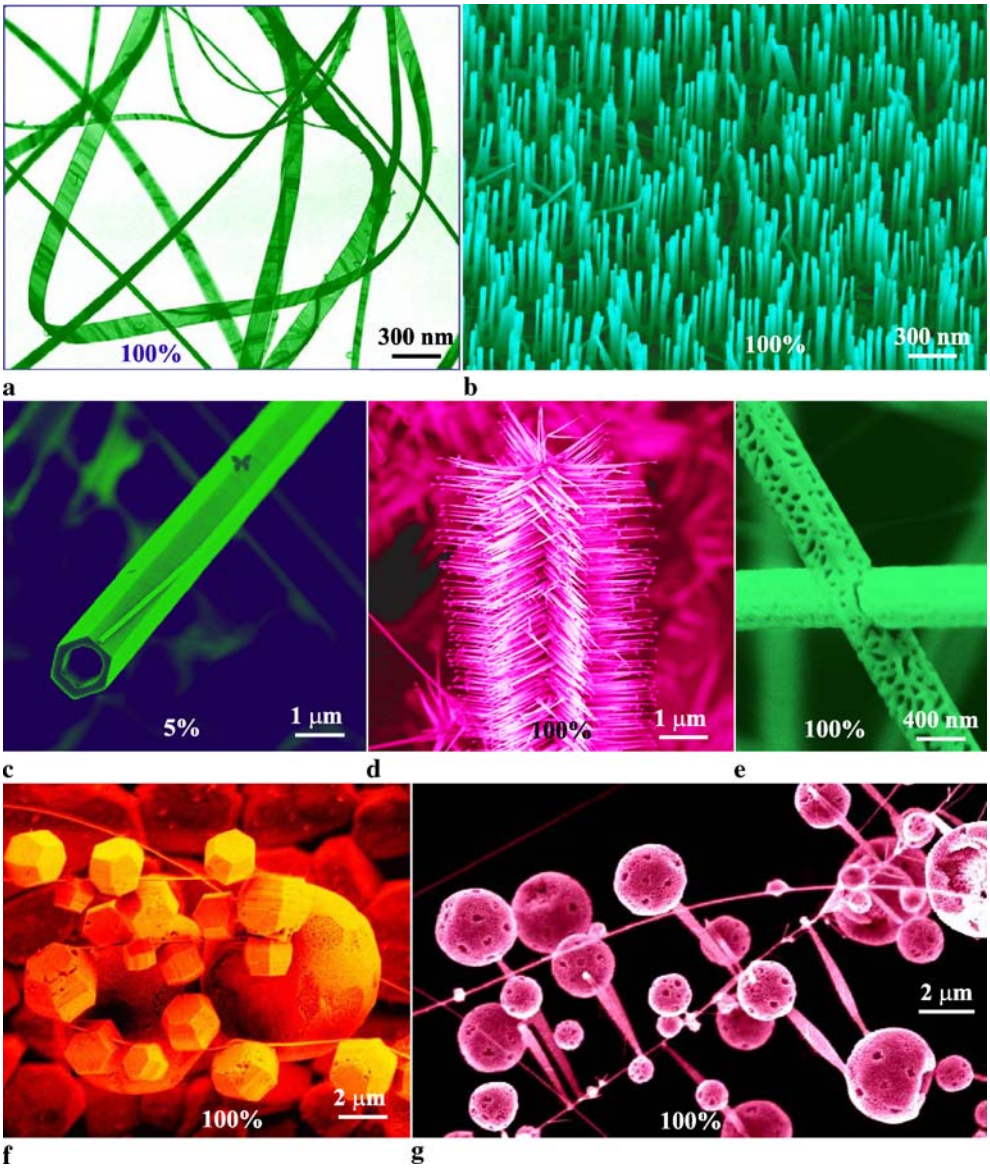

FIGURE 2 A collection of novel nanostructures of ZnO dominated by non-polar surfaces, synthesized under controlled conditions by thermal evaporation of solid powders by controlling source materials, growth temperature, temperature gradient and substrate. (**a**) Nanobelt; (**b**) aligned nanowire arrays; (**c**) nanotubes; (**c**) array of propellers; (**d**) mesoporous nanowires; (**e**) cages and shell structures; and (**f**) hierarchical shell and propeller structure. The percentage in each figure indicates the purity of the as-synthesized sample for the specific nanostructure in a specific local temperature region

polyhedron formed first during the solid–vapor phase growth. A subsequent oxidation of the Zn polyhedron forms a ZnO shell. Then, a sublimation of the Zn core results in the formation of the ZnO shell. A combination of the nanocages and the nanopropeller gives a hierarchical structure as shown in Fig. 2g [22].

3 Polar-surface-induced nanostructures

The synthesis of various nanostructures is based on a solid-state thermal sublimation process in which a pile of source materials, typically the powder form of oxides, is placed at the center of a tube furnace. The source materials are sublimated by raising the temperature; a redeposit ion of the vapor phase at a lower temperature zone gives some novel nanostructures. By controlling the growth kinetics, local growth temperature and the chemical composition of the source materials, a wide range of polar-surface dominated nanostructures of ZnO have been synthesized under well-controlled conditions at high yield (Fig. 3) [23, 24].

3.1 *Self-catalyzed growth on cation-terminated polar surface*

The cation-terminated polar surface is chemically active in the growth of nanostructures. The Zn-terminated (0001) surface, for example, is catalytically active, while the O-terminated $(000\bar{1})$ surface is inactive, resulting in the growth of saw-teeth structure (Fig. 3a) [25]. This growth structure has also been observed for ZnS and CdSe [26, 27]. With the formation of an inversion domain boundary along the central stem, both sides of the step can be terminated with Zn, leading to the growth of symmetric double-sided combs (Fig. 3l) [28]. By forming a multiply twinned octahedral core, fast growth along the [0001] results in the tetra leg structure (Fig. 3b) [29].

Using NaAOT as templates, hexagonal disks and rings of ZnO have been grown using a solution-based synthesis (Fig. 3c) [30]. The growth mechanism of the hexagonal disks is suggested due to the charge compensation of the anion AOT^- template at the Zn^{2+}-(0001) surface of ZnO; a fast

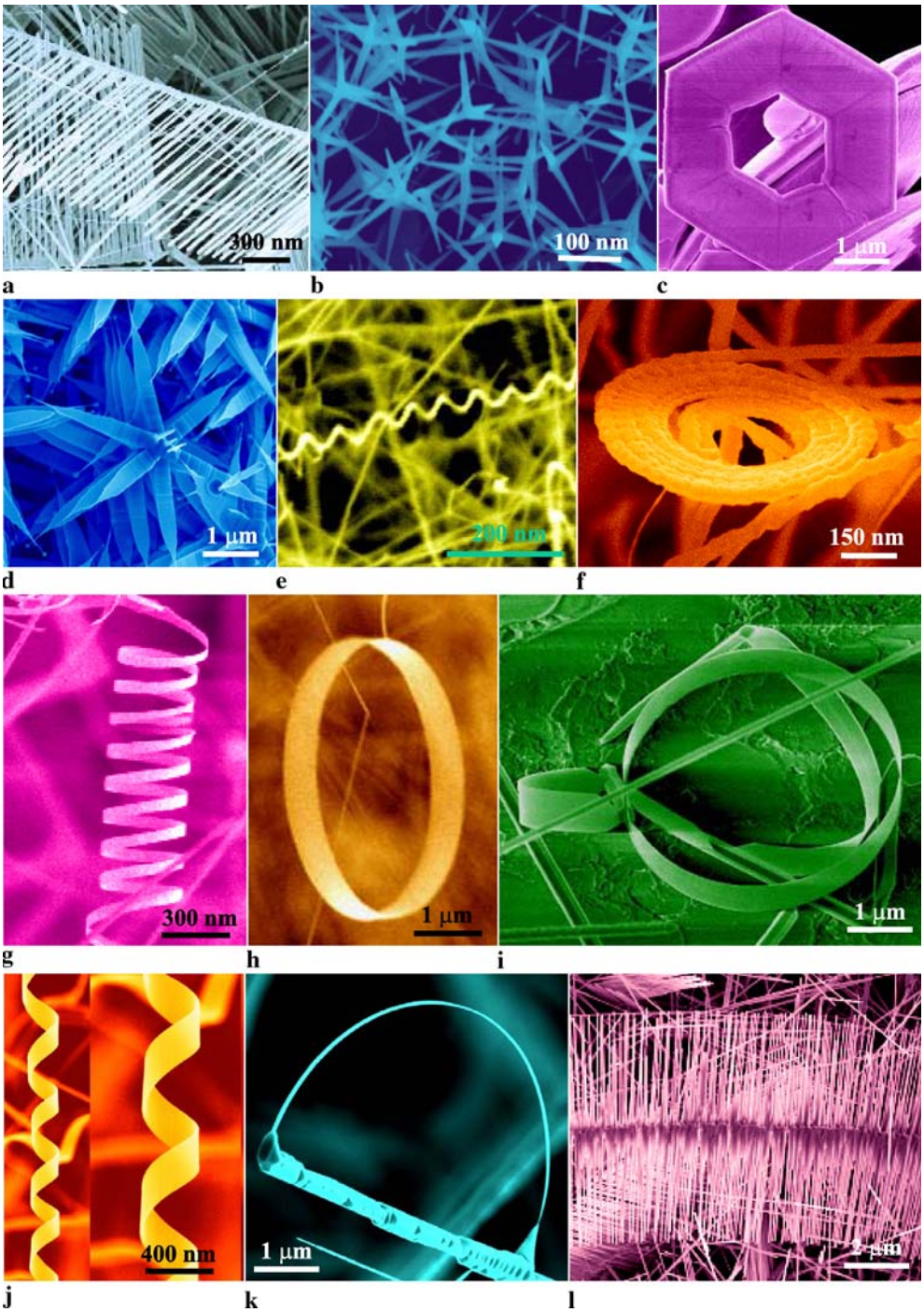

FIGURE 3 A collection of polar-surface-induced/dominated nanostructures of ZnO synthesized under controlled conditions by thermal evaporation of solid powders unless notify otherwise: (**a**) nanocombs induced by asymmetric growth on the Zn-(0001) surface; (**b**) tetraleg structure due to catalytically active Zn-(0001) surfaces; (**c**) hexagonal disks/rings synthesized by solution-based chemical synthesis; (**d**) nanopropellers created by fast growth along $\langle 01\bar{1}0\rangle$ and *c*-axis; (**e**) deformation-free nanohelixes as a result of block-by-block self-assembly; (**f**) spiral of a nanobelt with increased thickness along the length; (**g**) nanosprings; (**h**) single-crystal seamless nanoring formed by loop-by-loop coiling of a polar-nanobelt; (**i**) a nanoarchitecture composed of a nanorod, nanobow, and nanoring. The percentage in each figure indicates the purity of the as-synthesized sample for the specific nanostructure in a specific local temperature region. (**j**) Double-sided nanocombs formed with the presence of an inversion domain boundary parallel to the center stem and the symmetric teeth are the result of self-catalysis of Zn-termined (0001). (**k**) Nanobow structure produced by a change in growth direction from *c*-axis to *a*-axis. (**l**) Rigid helix of ZnO formed by superlattice structured nanobelt for reducing the surface energy of the polar surfaces

growth along $\langle 2\bar{1}\bar{1}0\rangle$ forms the hexagonal disks enclosed by the $\{10\bar{1}0\}$ facets. A higher density of defects at the center of the disk results in a higher local reaction/etching rate by NH_4^+ and NH_3. A thickness-through hole as defined by the $\{10\bar{1}0\}$ facets at the center leads to the formation of a hexagonal ring.

We used a mixture of ZnO and SnO_2 powders as the source material to grow a complex ZnO nanostructure [31, 32]. Figure 3d shows an SEM image of the as-synthesized products with a uniform feature consisting of sets of central axial nanowires. The growth of the novel structure presented here can be separated into two stages. The first stage is a fast growth of the ZnO axial nanowire along [0001]. The growth rate is so high that a slow increase in the size of the Sn droplet has little influence on the diameter of the nanowire, thus the axial nanowire has a fairly uniform shape along the growth direction. The second stage of the growth is the nucleation and epitaxial growth of the nanoribbons due to the arrival of the tiny Sn droplets onto the ZnO nanowire surface. The Sn liquid droplets deposited onto the ZnO nanowire lead to the simultaneous growth of the ZnO nanoribbons along the six equivalent growth directions: $\pm[10\bar{1}0]$, $\pm[0\bar{1}10]$ and $\pm[\bar{1}100]$. Secondary growth along [0001] results in the growth of the aligned nanowires on the surfaces of the propellers.

3.2 *Self-coiling of polar nanobelts/nanowires*

ZnO has two polar surfaces: {0001} and $\{01\bar{1}1\}$. The former is frequently observed, but the latter is rare. Recently, we have found that the ZnO nanowires dominated by $\{01\bar{1}1\}$ can form ultrasmall, deformation-free, single-crystal nanohelixes/nanosprings (Fig. 3e) [33]. The nanohelixes are made of $\sim$ 12 nm nanowires and have a uniform mean diameter of $\sim$ 30 nm. The growth follows a hexagonal screw-coiling model in which the growth of the nanowire is led by the Zn-terminated (0001) front surface due to self-catalysis. A sequential and periodic 60° rotation in growth direction among the six equivalent directions of $\langle 0\bar{1}11\rangle$ in an ordered and equally spaced distance results in the formation of the nanohelix. The sequential change in growth direction is to reduce the electrostatic interaction energy caused by the $\pm\{01\bar{1}1\}$ polar surfaces of the nanowire.

We have recently synthesized ZnO nanobelts that are dominated by the (0001) polar surface. The nanobelt grows along $[2\bar{1}\bar{1}0]$ (the *a*-axis), with its top/bottom surface $\pm(0001)$ and the side surfaces $\pm(01\bar{1}0)$. Due to the small thickness of 5–20 nm and large aspect ratio of $\sim$ 1:4, the flexibility and toughness of the nanobelts are both extremely high. From the model presented in Fig. 1b, {0001} are polar surfaces. A polar-surface-dominated nanobelt can be approximated to be a capacitor with two parallel charged plates. The polar nanobelt tends to roll over into an enclosed ring to reduce the electrostatic energy. A spiral shape is also possible for reducing the electrostatic energy (Fig. 3f) [34]. If the surface charges are uncompensated during the growth, the spontaneous polarization induces electrostatic energy due to the dipole moment, but rolling up to form a circular ring would minimize or neutralize the overall dipole moment (see Fig. 1c), reducing the electrostatic energy. On the other hand, bending of the nanobelt produces elastic energy. The stable shape of the nanobelt is determined by the minimization of the total energy contributed by spontaneous polarization and elasticity.

If the nanobelt is rolled uniradically loop-by-loop, the repulsive force between the charged surfaces stretches the nanohelix, while the elastic deformation force pulls the loops together; the balance between the two forms the nanospring (Fig. 3g) [34]. The nanohelix has a uniform shape with radius of $\sim$ 500–800 nm and evenly distributed pitches. Each is made of a uniformly deformed single-crystal ZnO nanobelt.

The nanohelixes and nanospirals are made of polar nanobelts whose polarization is perpendicular to the spiraling axis. If the polarization is rotated 90° and points parallel to the spiral axis, a seamless nanoring is formed through a loop-by-loop self-coiling process (Fig. 3h) [10]. The polar nanobelt, which is the building block of the nanoring, grows along $[10\bar{1}0]$, with side surfaces $\pm(1\bar{2}10)$ and top/bottom surfaces $\pm(0001)$, and have a typical width of $\sim$ 15 nm and thickness $\sim$ 10 nm. The nanobelt has polar charges on its top and bottom surfaces. If the surface charges are uncompensated during growth, the nanobelt may tend to fold itself as its length increases to minimize the area of the polar surface. One possible way is to interface the positively charged Zn-(0001) plane (top surface) with the negatively charged O-$(000\bar{1})$ plane (bottom surface), resulting in neutralization of the local polar charges and the reduced surface area, thus forming a loop with an overlapped end. The long-range electrostatic interaction is likely to be the initial driving force for folding the nanobelt to form the first loop for the subsequent growth. As the growth continues, the nanobelt may be naturally attracted onto the rim of the nanoring due to electrostatic interaction and extends parallel to the rim of the nanoring to neutralize the local polar charge and reduce the surface area, resulting in the formation of a self-coiled, co-axial, uni-radius, multi-looped nanoring structure. The reduced surface area and the formation of chemical bonds (short-range force) between the loops stabilize the coiled structure. A uni-radius and perfectly aligned coiling is energetically favorable because of the complete neutralization of the local polar charges inside the nanoring and the reduced surface area. This is a loop-by-loop self-coiling process of a nanobelt that is called the "slinky" growth model. The charge distributed on the surface of the coiling nanobelt is similar to the charge distribution on the RNA helix (see Fig. 1d).

Due to the three types of fastest growth directions: $\langle 0001\rangle$, $\langle 01\bar{1}0\rangle$, $\langle 2\bar{1}\bar{1}0\rangle$ and the polar surface induced phenomena, a diversity group of nanostructures has been grown for ZnO. The growth of several features can proceed simultaneously or one after the other, resulting in a unique nanoarchitecture (Fig. 3i). A simple rotation from the [0001] growth direction to an *a*-axis growth direction results in the formation of nanobows (Fig. 3k), which is also a result of reducing the electrostatic energy produced by the polar charges [35, 36].

3.3 *Rigid helix of superlattice structured* ZnO

A new structural configuration of ZnO was recently discovered in our laboratory, which is a rigid helical structure of ZnO that is made of a superlattice-structured nanobelt formed spontaneously in a vapor–solid growth process (Fig. 3j) [37]. The nanohelix is initiated from a single-crystal stiff-nanoribbon that is dominated by the *c*-plane polar surfaces. To reduce the surface energy of the polar surfaces, an abrupt structural transformation of the single-crystal polar nanoribbon into stripes of the superlattice-structured partial-polar nanobelt leads to the formation of a uniform and perfect nanohelix due to rigid structural alteration. The superlattice nanobelt is a periodic, coherent, epitaxial and parallel assembly of two alternating stripes of zinc oxide crystals oriented with their *c*-axes perpendicular to each other. The growth of the nanohelix is terminated by transforming the partial polar-surface-dominated nanobelt into a nonpolar-surface-dominated single-crystal nanobelt. Our data suggest that reducing the polar surfaces could be the driving force for forming the superlattice structure, and the rigid structural rotation/twist caused by the superlattice results in the initiation and formation of the nanohelix. The nanohelix has been manipulated and its elastic properties have been measured. The nanohelix is likely to be an ideal and unique structure for fabricating electromechanically-coupled nanoscale sensors, transducers, and resonators.

4 Properties and applications

For applications in nanotechnology, ZnO has three key advantages. First, it is semiconductor with a direct wide band gap of 3.37 eV and a large excitation binding energy (60 meV). It is an important functional oxide, exhibiting near-UV emission and transparent conductivity at room temperature and higher. Secondly, due to the non-central symmetry, it is piezoelectric, which is a key phenomenon in building electro-mechanical coupled sensors and transducers at nanoscale. The piezoelectric coefficient of a polar nanobelt is about three times that of the bulk [38], it is a candidate for nanoscale electromechanical coupling devices. Finally, ZnO could be bio-safe and biocompatible, and it can be used for biomedical applications without coating. With these three unique characteristics, ZnO could be one of the most important nanomaterials in future research and applications. The diversity of nanostructures presented here for ZnO should open many fields of research in nanotechnology (for a review see [15]).

4.1 *Luminescent property*

ZnO is recognized as a promising photonic material in the blue-UV region. Nanowires have been demonstrated as laser sources [39]. For investigation of quantum confinement effect, nanobelts of small sizes are required. We have recently grown ultrasmall nanobelts using a novel catalyst [40]. The ZnO nanobelts produced by the tin film catalyst are rather narrow, thin and uniform (Fig. 4a). The electron diffraction pattern and high-resolution TEM image show that the nanobelts grow along [0001], its top surfaces are $(2\bar{1}\bar{1}0)$ and the side surfaces are $(0\bar{1}10)$. The average diameter of the nanobelts is 5.5 nm, with a standard deviation of ± 1.5 nm. Photoluminescence (PL) measurements were performed at room temperature using an Xe lamp with an excitation wavelength of 330 nm (Fig. 4b). In comparison to the PL from nanobelts of an average width of ~ 200 nm, the 6-nm nanobelts have a 14-nm shift in the emission peak, which possibly indicates quantum effect due to reduced size of the nanobelts.

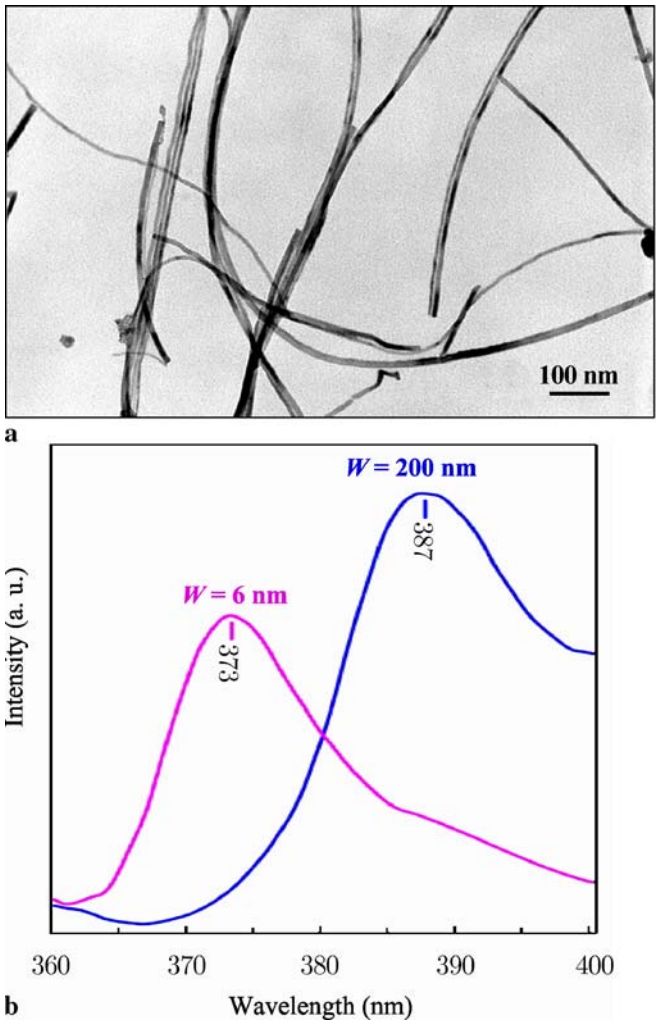

FIGURE 4 Ultra-narrow ZnO nanobelts. (**a**) TEM image of a ZnO nanobelts grown using tin thin film as the catalyst. (**b**) Photoluminescence spectra recorded from the wide nanobelts ($W = 200$ nm) and the narrow nanobelts ($W = 6$ nm), showing drastic blue shift in the emission peak due to size effect

4.2 *Field-effect transistor with tunable electrical properties*

Field-effect transistors have been fabricated using individual nanobelts [4]. An AFM image of the field-effect transistor (FET) and the schematic diagram is inserted in Fig. 5. The principle of this device is that controlling the gate voltage would control the current flowing from the source to the drain. The FET fabricated using an as-synthesized nanobelt behaves like a semiconductor device in air. But the conductivity of a nanobelt can be tuned by controlling its surface and volume oxygen deficiency. Before electrical measurement, SnO_2 nanobelts are annealed in 1 atm oxygen environment at 800 °C for 2 h. Without this treatment, the as-produced nanobelts exhibit no measurable conductivity for source-drain biases from -10 V to 10 V and for gate biases from -20 V to 20 V, while after this treatment the SnO_2 nanobelts exhibit considerable conductivity. By further annealing of the devices at lower temperatures in vacuum, oxygen, or ambient the electrical properties of the nanobelts, can be tuned. The strong dependence of the conductance on the oxygen deficiency in nanobelts is an important characteristic of functional oxide, which one is capable of tuning and controlling the electrical properties of the nanodevice.

4.3 *4.3 Photoconductivity*

Ultraviolet light irradiation of the nanobelt diode of ZnO in air results in a significant increase of the conductivity (Fig. 6). Light with a wavelength of 350 nm ($E_\lambda = 3.54$ eV) was used, exceeding the direct bandgap of ZnO. The increase in the conductivity results from both photogeneration of electron–hole pairs as well as doping by UV light-induced surface desorption [41–43]. These processes could be observed by introducing a shutter between the light source and the ZnO nanobelt so that the flux of UV photons could be turned 'ON' and 'OFF'.

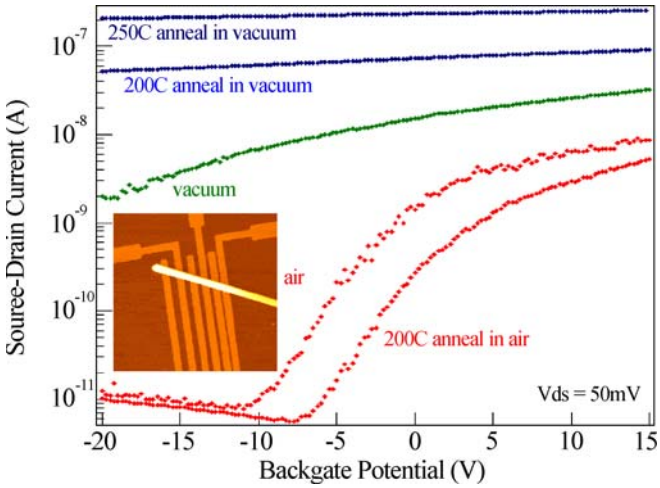

FIGURE 5 Field-effect transistor fabricated using a single SnO nanobelt and its *I–V* characteristics, depending on the environment and specimen treatment. The *inset* is an AFM image of the FET device

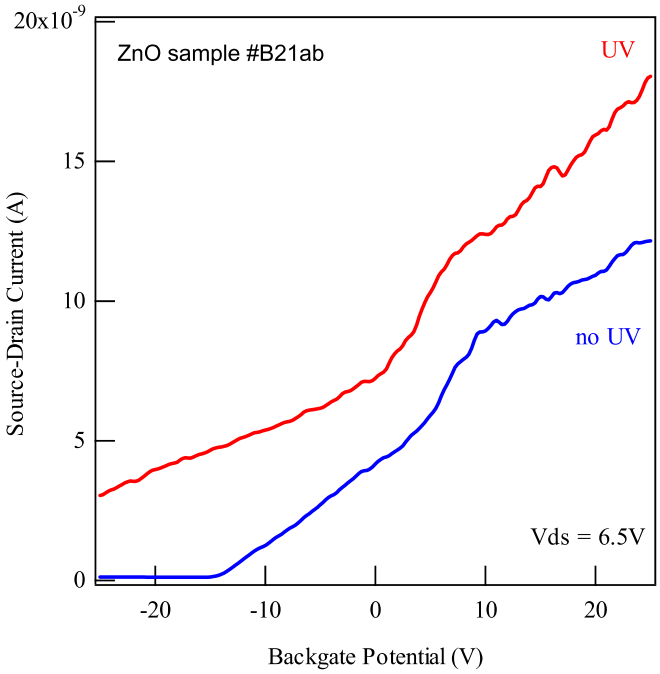

FIGURE 6 UV light stimulated current increase in an FET fabricated using a single ZnO nanobelt

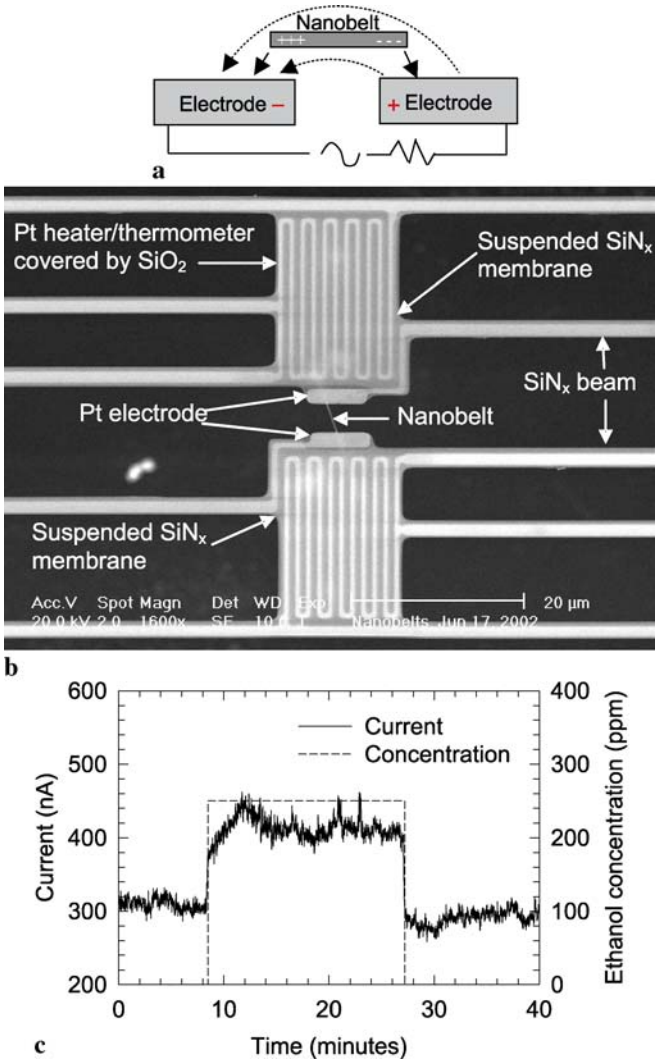

FIGURE 7 Integration of a nanobelt with a pre-fabricated MEMS. (**a**) Electrostatic-field-induced self-assembly of a nanobelt across two electrodes. (**b**) A pre-fabricated MEMS after integrating with one nanobelt. (**c**) Sensitivity of the current through the nanobelt as it is exposed to ethanol, demonstrating electric signal based device for in-situ, wireless chemical and possibly biochemical sensing (from Yu et al.[44])

4.4 *Gas, chemical, and biosensors*

Conductometric metal-oxide semiconductor thin films are the most promising devices among solid-state chemical sensors due to their small dimension, low cost, low power consumption, on-line operation and high compatibility with microelectronic processing. The fundamental sensing mechanism of metal-oxide-based gas sensors relies on a change in electrical conductivity due to the interaction process between the surface complexes such as O^-, O_2^-, H^+ and OH^- reactive chemical species and the gas molecules to be detected.

A key step in fabricating the single-belt-based sensor is the manipulation process and its integration with the pre-fabricated electrodes. An electric field-directed assembly method was demonstrated by Yu et al. [44]. In this method, an electrode pair in the micromechanical system (MEMS) device is connected to an ac voltage source. As a solution containing the nanobelts is dispersed on the surface of the MEMS array, the frequency of the ac field can be adjusted to generate an attractive force on the nanobelts that are polarized in the electric field (Fig. 7a). This phenomenon is called positive dielectrophoresis, where a polarizable particle in a non-uniform ac electric field is attracted to regions of high field strength. The attractive or positive dielectrophoretic force can be used to align and trap a nanobelt to an electrode pair.

The MEMS device was originally designed for measuring the thermal and thermoelectric properties of 1D nanostructures[8]. As shown in Fig. 7b, it consists of two adjacent silicon nitride (SiN_x) membranes supported by long SiN_x beams. A serpentine platinum (Pt) resistance thermometer (RT) is patterned on each membrane. The RT can be Joule heated used to increase the operating temperature of the sensor as well as to monitor the sensor temperature. Two sep-

arate parallel Pt electrodes are patterned on the two membranes, forming an electrode pair for trapping the nanobelt. A single SnO_2 nanobelt has been trapped on the Pt electrode pair of the MEMS device. Figure 7c shows the sensor response to 250 ppm ethanol balanced in air when the device was Joule heated to 400 °C. While the NO_2 gas depletes electrons by forming NO^{2-} on the sensor surface, OH^- group in the ethanol gas desorbs oxygen ions from the nanobelt and thereby enhance electrical conductance, leading to an increase in current soon after the ethanol gas was introduced to the chamber.

4.5 *Piezoelectricity of the polar nanobelts*

Piezoelectricity is due to the atomic-scale polarization. To illustrate the piezoelectricity, one considers an atom with a positive charge that is surrounded tetrahedrally by anions (Fig. 8a). The center of gravity of the negative charges is at the center of the tetrahedron. By exerting pressure on the crystal along the cornering direction of the tetrahedron, the tetrahedron will experience distortion, and the center of gravity of the negative charges will no longer coincide with the position of the positive central atom, an electric dipole is generated. If all of the tetrahedra in the crystal have the same orientation or some other mutual orientation that does not allow for a cancellation among the dipoles, the crystal will have a macroscopic dipole. The two opposite faces of the crystal have opposite electric charges.

The piezoelectric coefficient of ZnO nanobelt has been measured by atomic force microscopy using a conductive tip [45]. After coating (100) Si wafer with a 100 nm Pd, ZnO nanobelts were dispersed on the conductive surface. Then the whole surface was coated with another 5-nm Pd coating, which served as an electrode on ZnO nanobelt to get uniform electric field and avoid electrostatic effect. Extra care was taken to ensure that the top and bottom surface of the nanobelt was not short-circuited after Pd deposition. The ZnO nanobelt was located by a commercially available AFM under tapping mode. Piezoresponse force microscopy (PFM) is used to measure the effective piezoelectric coefficient (d_{33}) of individual (0001) surface dominated zinc oxide nanobelt lying on conductive surface. Based on references of bulk (0001) ZnO and x-cut quartz, effective piezoelectric coefficient d_{33} of ZnO nanobelt is found to be frequency dependent and varies from 14.3 pm/V to 26.7 pm/V (Fig. 8b), which is much larger than that of the bulk (0001) ZnO of 9.93 pm/V. The results project the applications of ZnO nanobelts as nanosensors and nanoactuators.

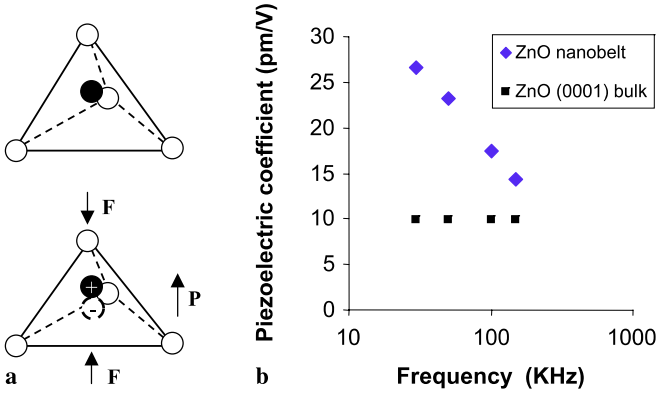

FIGURE 8 (**a**) Schematics showing piezoelectric effect in tetrahedrally coordinated cation-anion unit. (**b**) Experimentally measured piezoelectric coefficient d_{33} for ZnO and its comparison to that of the bulk

5 Summary

Nanostructures of functional oxides are splendid, diverse, and complex. This paper mainly focuses on the nanostructures of ZnO, which is a material of semiconducting, piezoelectricity, and pyroelectricity. Understanding their growth and properties is important for controlled synthesis and technological applications. The nanobelts and relevant nanostructures have potential applications in nanosize electronic, optical, sensor, resonator, and optoelectronic devices. To reach these goals, innovative research has to be carried out in the following areas:

1. Large-scale, high-yield growth is a key for industrial applications. Most of the current research is in the laboratory, thus, scaling-up and improving the yield are the first step.
2. Designed and controlled growth is required to control the size, size distribution, shape, and location of the nanostructures for direct integration with pre-fabricated electrodes.
3. Self-assembly and manipulation of nanostructures by chemical and physical techniques are required for parallel integration of the nanostructures with microsystems.
4. Functionalization of the surfaces of the oxide nanostructure is essential for improving its sensitivity and selectivity for chemical and biological sensing.
5. Fabrication of novel devices using the advantages offered by the geometry and properties of the nanostructures will be the essential task of the near future research.
6. Bio-compatibility and bio-safety of the nanostructures need to be extensively investigated.
7. The sustained interest in ZnO nanostructures will depend on their unique properties and high-yield, high-purity, and large-scale synthesis. We have recently made some progress towards manufacturing of aligned ZnO nanowires by exploring the phase diagram and road maps for controlled synthesis [46, 47]. This could be an important step towards nanomanufacturing.

ACKNOWLEDGEMENTS The results reviewed in this paper were partially contributed from our group members and collaborators: X.Y. Kong, X.D. Wang, P.X. Gao, Yong Ding, X.D. Bai, W. Hughes, R.S. Yang, C. Ma, C. Yu, Li Shi, M.S. Arnold, Ph. Avouris, Enge Wang, M.H. Zhao, S.X. Mao, Y. Dai and Y. Zhang, to whom we are very grateful. Research supported by NSF, NASA, and DARPA.

REFERENCES

1 Z.W. Pan, Z.R. Dai, Z.L. Wang, Science **291**, 1947 (2001)
2 Z.L. Wang (ed.), *Nanowires and Nanobelts, Vol. I: Metal and Semiconductor, Nanowires* (Kluwer Academic Publishers, Dordrecht, 2003)
3 Z.L. Wang (ed.), *Nanowires and Nanobelts, Vol. II: Nanowires and Nanobelts of Functional Materials* (Kluwer Academic Publishers, Dordrecht, 2003)
4 M.S. Arnold, P. Avouris, Z.W. Pan, Z.L. Wang, J. Phys. Chem. B **107**, 659 (2002)

5 E. Comini, G. Faglia, G. Sberveglieri, Z.W. Pan, Z.L. Wang, Appl. Phys. Lett. **81**, 1869 (2002)
6 X.D. Bai., P.X. Gao, Z.L. Wang, E.G. Wang, Appl. Phys. Lett. **82**, 4806 (2003)
7 W.L. Hughes, Z.L. Wang, Appl. Phys. Lett. **82**, 2886 (2003)
8 L. Shi, Q. Hao, C. Yu, D. Kim, N. Mingo, X.Y. Kong, Z.L. Wang, Appl. Phys. Lett. **84**, 2638 (2004)
9 X.Y. Kong, Z.L. Wang, Nano Lett. **3**, 1625 (2003)
10 X.Y. Kong, Y. Ding, R. Yang, Z.L. Wang, Science **303**, 1348 (2004)
11 Z.L. Wang, Z.C. Kang, *Functional and Smart Materials – Structural Evolution and Structure Analysis* (Plenum Publishing Co., New York, 1998)
12 S.C. Minne, S.R. Manalis, C.F. Quate, Appl. Phys. Lett. **67**, 3918 (1995)
13 See the special issue on transparent conducting oxides, MRS Bulletin, August issue (2000), published by Materials Research Society
14 C.R. Gorla, N.W. Emanetoglu, S. Liang, W.E. Mayo, Y. Lu, M. Wraback, H. Shen, J. Appl. Phys. **85**, 2595 (1999)
15 Z.L. Wang, Ann. Rev. Phys. Chem. **55**, 159 (2003)
16 Z.L. Wang, J. Phys.: Condens. Matter **16**, 829 (2004)
17 X.D. Wang, C.J. Summers, Z.L. Wang, Nano Lett. **3**, 423 (2004)
18 P.X. Gao, C.S. Lao, Y. Ding, Z.L. Wang, Adv. Funct. Mater. **16**, 53 (2006)
19 P.X. Gao, Z.L. Wang, Appl. Phys. Lett. **84**, 2883 (2004)
20 X.D. Wang, C.J. Summers, Z.L. Wang, Adv. Mater. **16**, 1215 (2004)
21 P.X. Gao, Z.L. Wang, J. Am. Chem. Soc. **125**, 11 299 (2003)
22 R.S. Yang, Z.L. Wang, unpublished result (2007)
23 Z.L. Wang, Mater. Today **7**, 26 (2004)
24 Z.L. Wang, X.Y. Kong, Y. Ding, P.X. Gao, W. Hughes, R.S. Yang, Y. Zhang, Adv. Funct. Mater. **14**, 944 (2004)
25 Z.L. Wang, X.Y. Kong, J.M. Zuo, Phys. Rev. Lett. **91**, 185 502 (2003)
26 D. Moore, C. Ronning, C. Ma, L. Wang, Chem. Phys. Lett. **385**, 8 (2004)
27 C. Ma, Y. Ding, D. Moore, X.D. Wang, Z.L. Wang, J. Am. Chem. Soc. **126**, 708 (2004)
28 C.S. Lao, P.X. Gao, R.S. Yang, Y. Zhang, Y. Dai, Z.L. Wang, Chem. Phys. Lett. **417**, 359 (2005)
29 Y. Dai, Y. Zhang, Z.L. Wang, Solid State Commun. **126**, 629 (2003)
30 F. Li, Y. Ding, P.X. Gao, X.Q. Xin, Z.L. Wang, Angew. Chem. Int. Edit. **116**, 5350 (2004)
31 P.X. Gao, Z.L. Wang, J. Phys. Chem. B **106**, 12 653 (2002)
32 P.X. Gao, Z.L. Wang, Appl. Phys. Lett. **84**, 2883 (2004)
33 R.S. Yang, Y. Ding, Z.L. Wang, Nano Lett. **4**, 1309 (2004)
34 X.Y. Kong, Z.L. Wang, Appl. Phys. Lett. **84**, 975 (2004)
35 W.L. Hughes, Z.L. Wang, J. Am. Chem. Soc. **126**, 6703 (2004)
36 W.L. Hughes, Z.L. Wang, Appl. Phys. Lett. **86**, 043 106 (2005)
37 P.X. Gao, Y. Ding, W.J. Mai, W.L. Hughes, C.S. Lao, Z.L. Wang, Science **309**, 1700 (2005)
38 M.H. Zhao, Z.L. Wang, S.X. Mao, Nano Lett. **4**, 587 (2004)
39 M.H. Huang, S. Mao, H. Feick, H.Q. Yan, Y.Y. Wu, H. Kind, E. Weber, R. Russo, P.D. Yang, Science **292**, 1897 (2001)
40 X.D. Wang, Y. Ding, C.J. Summers, Z.L. Wang, J. Phys. Chem. B **108**, 8773 (2004)
41 D.H. Zhang, Mater. Chem. Phys. **45**, 248 (1996)
42 P. Bonasewicz, W. Hirschwald, G. Neumann, J. Electrochem. Soc. **133**, 2270 (1986)
43 Y. Shapira, S.M. Cox, D. Lichtma, Surf. Sci. **54**, 43 (1976)
44 C. Yu, Q. Hao, S. Saha, L. Shi, X.Y. Kong, Z.L. Wang, Appl. Phys. Lett. **86**, 063 101 (2005)
45 M.H. Zhao, Z.L. Wang, S.X. Mao, Nano Lett. **4**, 587 (2004)
46 J.H. Song, X.D. Wang, E. Riedo, Z.L. Wang, J. Phys. Chem. B **109**, 9869 (2005)
47 C. Ma, Z.L. Wang, Adv. Mater. **17**, 1 (2005)